Accepted for publication in *Landscape and Urban Planning* on October 1, 2016

Simulating the cooling effects of water spray systems in urban landscapes: A computational fluid dynamics study in Rotterdam, the Netherlands

H. Montazeri*[,1,2], Y. Toparlar[2,3], B. Blocken[1,2], J.L.M. Hensen[2]

1 Building Physics Section, Department of Civil Engineering, KU Leuven, Kasteelpark Arenberg 40 – bus 2447, 3001 Leuven, Belgium
2 Building Physics and Services, Department of the Built Environment, Eindhoven University of Technology, P.O. box 513, 5600 MB Eindhoven, The Netherlands
3 Environmental Modeling, Flemish Institute for Technological Research, Mol, Belgium

Graphical abstract

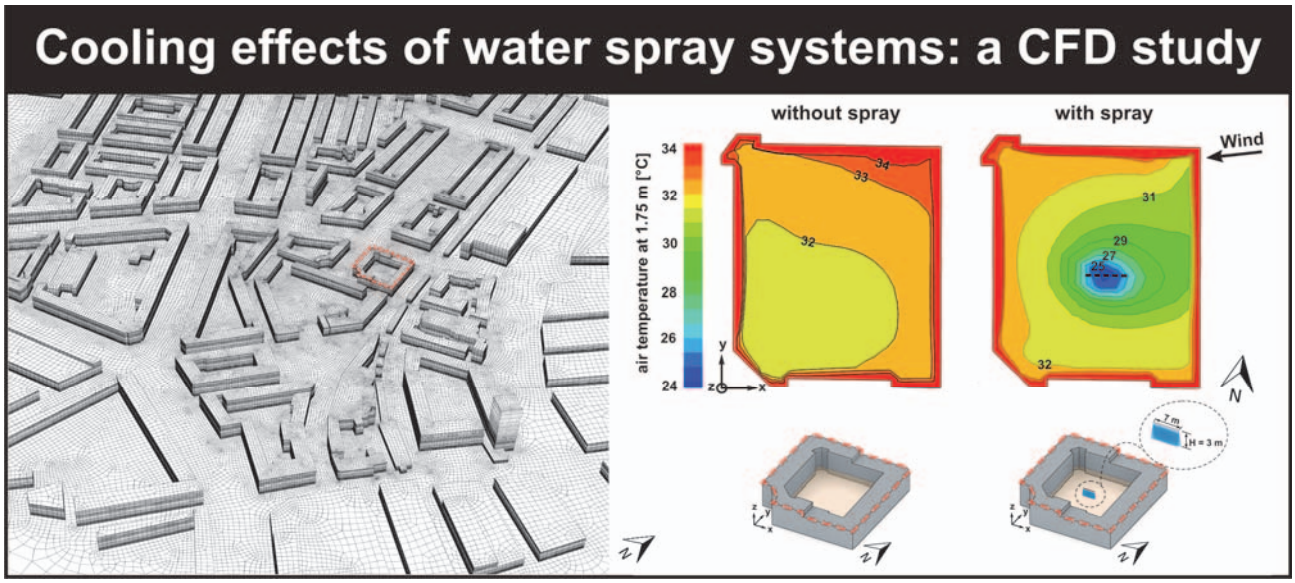

Research highlights:

- Water spraying is an effective measure for improving outdoor thermal comfort
- Maximum air temperature reduction and UTCI reduction are 5 and 7 °C at 1.75m height
- Thermal comfort at pedestrian height is improved up to 5 m away from spray system
- Water flow rate and spray height strongly affect cooling potential of spray systems

* Corresponding author: Hamid Montazeri, Building Physics Section, Department of Civil Engineering, KU Leuven, Kasteelpark Arenberg 40 – bus 2447, 3001 Leuven, Belgium. Email address: hamid.montazeri@kuleuven.be

Accepted for publication in *Landscape and Urban Planning* on October 1, 2016

Simulating the cooling effects of water spray systems in urban landscapes: A computational fluid dynamics study in Rotterdam, the Netherlands

H. Montazeri[*,1,2], Y. Toparlar[2,3], B. Blocken[1,2], J.L.M. Hensen[2]

1 Building Physics Section, Department of Civil Engineering, KU Leuven, Kasteelpark Arenberg 40 – bus 2447, 3001 Leuven, Belgium
2 Building Physics and Services, Department of the Built Environment, Eindhoven University of Technology, P.O. box 513, 5600 MB Eindhoven, The Netherlands
3 Environmental Modeling, Flemish Institute for Technological Research, Mol, Belgium

Abstract: Heat waves and the related heat stress can increase human morbidity and mortality, decrease human productivity and increase building energy consumption for cooling. There is a need for sustainable systems to reduce heat stress in urban areas. Evaporative cooling by water spray systems is increasingly used for this purpose. However, the evaluation of the cooling potential of such systems is difficult. To our knowledge, a systematic investigation of the cooling potential of such a system in an actual urban area has not yet been performed. This paper presents high-resolution Computational Fluid Dynamics (CFD) simulations based on the 3D unsteady Reynolds-Averaged Navier-Stokes equations to assess the cooling potential by a water spray system with 15 hollow-cone nozzles. The system is numerically implemented for a courtyard in the Bergpolder Zuid region of Rotterdam, the Netherlands and operated during the heat wave period of July 2006. The simulations are validated based on wind-tunnel measurements of an evaporative cooling process and satellite imagery data during the heat wave period. The Universal Thermal Climate Index (UTCI) is used to assess the heat stress reduction due to evaporative cooling. The results show that for given values of injected water flow rate ($\dot{m}_w$ = 9.0 l/min) and height of the spray system (H = 3 m), a maximum temperature reduction and UTCI reduction of about 7 and 5°C are achieved at pedestrian height. In addition, a thermal comfort improvement from strong heat stress (without spray system) to moderate heat stress up to a distance of 5m from the spray line is obtained.

Keywords: Urban microclimate; urban physics; climate change adaptation; thermal comfort; built environment

1 Introduction

Climate change is expected to increase the frequency and the intensity of heat waves (Kovats and Hajat, 2008). Major heat waves, such as the European heat waves of 2003 and 2006, might occur more frequently and could become common events by 2040 (Kovats and Hajat, 2008; Stott et al., 2004). Increased heat waves and heat stress will cause increased heat-related morbidity and mortality, as illustrated for the hot summers of 2003 and 2006 (Fischer et al., 2004; Haines et al., 2006). During the summer of 2003, more than 70,000 heat-related deaths were reported in Europe (Robine et al., 2008). Due to increased intensity and frequency of heat waves, cooling energy demand in summer is expected to increase by 72% worldwide by 2100 (Isaac and Van Vuuren, 2009). These problems are potentially aggravated by the urban heat island effect (UHI) (Oke, 1982; Grimmond and Oke, 1991; Mirzaei and Haghighat, 2010; Allegrini et al., 2012; Heusinkveld et al., 2013).

Several urban scale adaptation measures, such as vegetation, increased short-wave reflectivity of surfaces and evaporative cooling can be employed to decrease high temperatures in urban areas (Akbari et al., 1997; Gromke et al., 2015; Rizwan et al., 2008; Rosenfeld et al., 1995). Among the proposed measures, the use of water spray systems for evaporative cooling is becoming more popular (Huang et al., 2011; Sureshkumar et al., 2008a). Water spraying can be an effective and economical tool for improving both indoor and outdoor thermal comfort. Most available adaptation measures such as vegetation and increased short-wave reflectivity are so-called passive systems, which normally have effects all year long with little or no controllability. While they clearly can provide positive effects during warm seasons, they may lead to increased building energy consumption in the winter season. (Loonen et al., 2013; Taleghani et al., 2014; van Hooff et al., 2014, 2016). Water spray systems, on the other hand, are flexible in use with dynamic controls and can be easily integrated in various projects (Pearlmutter et al., 1996).

The two-phase flow in water spray systems is very complex as the evaporation process depends on several physical parameters, which are not easily varied independently (Ashgriz, 2011; Lefebvre, 1989; Montazeri et al., 2015a, 2015b). Given the complexities involved in evaluating the performance of water spray systems, most previous studies were

* Corresponding author: Hamid Montazeri, Building Physics Section, Department of Civil Engineering, KU Leuven, Kasteelpark Arenberg 40 – bus 2447, 3001 Leuven, Belgium. Email address: hamid.montazeri@kuleuven.be

performed using field measurements. They evaluated the influence of different physical parameters on the performance of water spray systems, such as ambient air temperature and air humidity (Huang et al., 2011; Nishimura et al., 1998), solar radiation (Takahashi et al., 2010), elapsed time under influence of spray (Farnham et al., 2015) and nozzle spray characteristics. However, field measurements are usually only performed in a limited number of points in space. In addition, there is almost no or limited control over the boundary conditions. This is, however, very important given the wide range of parameters influencing the performance of evaporative cooling systems.

Numerical simulation by Computational Fluid Dynamics (CFD) can be a useful tool to investigate the two-phase flow in spray systems. The use of CFD for the evaluation of urban meteorology and microclimate has seen a rapid growth in the past 50 years (Blocken, 2014). This growth has been strongly supported by the development of best practice guidelines for CFD applications for urban areas (Blocken, 2015; Casey and Wintergerste, 2000; Franke et al., 2007; Tominaga et al., 2008) and is illustrated by a large number of review, overview and position papers (e.g. (Blocken, 2015, 2014; Blocken and Carmeliet, 2004; Mochida and Lun, 2008; Murakami, 1997; Murakami et al., 1999; Ramponi and Blocken, 2012; Stathopoulos, 2002, 1997; Tominaga and Stathopoulos, 2013; Toparlar et al., 2015)). As a result, CFD is increasingly used to evaluate the potential of sustainable and renewable energy systems (e.g. (Calautit et al., 2013; Montazeri, 2011; Montazeri et al., 2010; Montazeri and Azizian, 2009)), including the cooling performance of water spray systems (Kang and Strand, 2013; Montazeri et al., 2015a, 2015b; Sureshkumar et al., 2008b). However, to our knowledge, a systematic investigation of the cooling potential of water spray systems in an actual urban area has not yet been performed. Therefore, the current paper presents CFD simulations on a high-resolution grid to assess the cooling potential of a water spray system with hollow-cone nozzles for a courtyard in the Bergpolder Zuid region of the Dutch city of Rotterdam, the Netherlands in July 2006, when one of the major European heat waves occurred. In addition, the impact of the injected water flow rate and the height of the spray system on its cooling performance is investigated.

In Section 2, the Bergpolder Zuid region is described. Section 3 presents the validation study for the evaporative cooling model. In Section 4, the CFD simulations for Bergpolder Zuid are outlined. Section 5 presents a parametric analysis for evaporative cooling in Bergpolder Zuid. Finally, discussion (Section 6) and conclusions (Section 7) are provided.

2 Urban area and surroundings

Following the reports of the Intergovernmental Panel on Climate Change (IPCC), more and more research organizations and consortia have started to focus on climate adaptation (Parry et al., 2007). One of these was the Climate Proof Cities (CPC) research consortium composed of universities, research institutes, policy makers and city officials investigating the application of urban scale adaptation measures in the Netherlands (Albers et al., 2015). One of the focus areas was the Bergpolder Zuid region in Rotterdam, located in the Noord district of the city (Fig. 1).

Rotterdam is subjected to an oceanic climate influenced by the Atlantic Ocean and the North Sea, which is similar in the rest of the country. Based on the Köppen-Geiger classification (Strahler and Strahler, 1984), the climate of the Netherlands is Cfb, a climate with moderate winters and moderately warm summers, though heat waves are becoming more and more frequent.

The Bergpolder Zuid region consists of both residential and office buildings with narrow streets and surrounded by large avenues (Fig. 1c). Most of the streets in the region are narrow with an aspect ratio between 1:1 and 2:1. Note that the aspect ratio is defined here as the ratio of the adjacent building height to the street width. The average building height is about 12.6 m where the lowest building is 2.8 m and the highest building is 51.0 m. No significant vegetation or water bodies are present in the region.

The Bergpolder Zuid region is bordered by the central district of Rotterdam in the south and mainly green fields to the north, until the city of Delft (located in the northwest). Based on the updated Davenport roughness classification (Wieringa, 1992), the aerodynamic roughness length (z_0) of the surroundings, which is necessary as input for the CFD simulations, is determined as shown in Fig. 2. The z_0 value is determined as a spatial average of the z_0 values of the different patches of roughness (land use) of the terrain within a 10 km radius upstream of the urban area (Fig. 2).

3 Evaporative cooling validation study

Due to lack of high-resolution experimental data for water spray systems in urban areas, the wind-tunnel measurements of dry-bulb temperature (DBT) and wet-bulb temperature (WBT) during evaporative cooling by a hollow-cone nozzle spray system by Sureshkumar et al. (Sureshkumar et al., 2008a) are used for CFD validation. Because this validation study has been published as a separate paper (Montazeri et al., 2015a), only the headlines are briefly repeated here.

3.1. Wind-tunnel measurements

The measurements were conducted in an open-circuit wind tunnel with a test section of 1.9 m length and a cross-section of 0.585×0.585 m^2 (Fig. 3). A uniform approach-flow mean wind speed was employed. The inlet air dry-bulb temperature (DBT) and wet-bulb temperature (WBT) were measured by two thermocouples placed upstream of the spray nozzle. The outlet DBT and WBT variations were recorded with thermocouples at nine positions across the outlet plane of the test section (Fig. 3). The inlet and outlet water temperatures were obtained with two thermocouples upstream of the nozzle

and at the outlet plane, respectively. A pressure gauge was also installed upstream of the nozzle to monitor the water pressure.

The impact of nozzle opening on the cooling performance of the spray system was evaluated with four nozzles with different discharge openings of 3, 4, 5 and 5.5 mm. Each nozzle was installed in the middle of a cross-section of the test section and designed in a way that the exiting water forms a hollow-cone sheet disintegrating into droplets. The droplet diameter distribution was determined using an image-analyzing technique. The experiments were conducted for 36 cases; four different nozzle discharge diameters (i.e. D = 3, 4, 5 and 5.5 mm), three inlet nozzle gauge pressures (P = 1, 2 and 3 bar) and three inlet air velocity values (V = 1, 2 and 3 m/s). The inlet water temperature, T_{in}, varied between 33 and 36 °C for all cases. The cases with nozzle discharge diameter of 4 mm and gauge pressure P = 3 bar are withheld for the validation study since droplet size distribution data are also available for these cases. A list of some main parameters of these cases, including the half-cone angle, $\alpha/2$, and the inlet water flow rate, $\dot{m}_w$, is presented in Table 1.

3.2. CFD simulations and validation

A 3D computational domain representative of the wind-tunnel test section is generated. The domain has a width, height and length of 0.585 m, 0.585 m and 1.9 m, respectively. The geometry and the computational grid are generated using the commercial Gambit 2.4.6 software. The resulting grid has 1,018,725 hexahedral cells. More information is provided in Ref. (Montazeri et al., 2015a).

In the simulations, the mean velocity inlet boundary condition for the continuous phase is a uniform profile according to the measured data (= U_∞). As the turbulence characteristics of the flow were not reported in (Sureshkumar et al., 2008a), a turbulence intensity, I, of 10% is assumed for the inlet flow, which is relevant for practical applications and for atmospheric boundary layer wind flow. The turbulent kinetic energy k is calculated from U_∞ and I using Eq. (1). The turbulence dissipation rate, ε, is given by Eq. (2). The turbulence length scale, l (m), in this equation is taken as $l = 0.07D_H$ where D_H is the hydraulic diameter of the domain which is equal to the width of the test section (= 0.585 m).

$$k = (U_\infty . I)^2 \tag{1}$$

$$\varepsilon = C_\mu^{3/4} \frac{k^{3/2}}{l} \tag{2}$$

A constant temperature equal to the measured DBT is imposed at the inlet. A fixed vapor mass fraction is also calculated based on the experimental data and imposed at the inlet as a boundary condition for the vapor transport equation. The vapor mass fraction for the moist air can be taken as x/(x+1) where x ($kg_{vapour}/kg_{dry\text{-}air}$) is the humidity ratio of air. The walls of the computational domain are modeled as no-slip walls with zero equivalent sand-grain roughness height $k_S = 0$ m in the roughness modification of the wall functions (Cebeci and Bradshaw, 1977). The standard wall functions by Launder and Spalding (Launder and Spalding, 1974) are applied. The adiabatic thermal boundary condition is used for these surfaces. Zero static gauge pressure is applied at the outlet plane.

For impinging drops, the so-called "reflected" boundary condition is imposed at the walls. For the outlet plane, the "escape" boundary condition is considered where the droplets leave the domain with their current conditions (i.e. velocity, temperature and vapor mass fraction at the outlet plane) and trajectory calculations are terminated (ANSYS Inc., 2009).

The size distribution of the droplets is described by the Rosin-Rammler model (Rosin and Rammler, 1933). For the current experimental data, $\overline{D}$ and n are 369 μm and 3.67, respectively (Montazeri et al., 2015a). The smallest droplet diameter to be considered in the size distribution of the Rosin-Rammler model is 74 μm, corresponding to the minimum resolution of the droplet measurements. The largest droplet diameter is 518 μm, based on the largest droplet diameter in the samples (Sureshkumar et al., 2008a). 20 discrete droplet diameters, N_D, are assumed to be injected from each droplet stream into the domain. The droplet diameters are distributed at equally spaced intervals of $(D_{max}\text{-}D_{min})/N_D$. The spherical drag law provided by Morsi and Alexander (Morsi and Alexander, 1972) is used to estimate the drag coefficients acting on the droplets.

The water droplets are injected into the computational domain using a virtual 4 mm diameter nozzle positioned in the middle of the inlet plane of the domain and oriented horizontally in the downstream direction. The total mass flow rate and temperature of the injected water droplets are imposed according to the experimental data (Table 1). The hollow cone spray model provided by ANSYS/Fluent 12.1 (ANSYS Inc., 2009) is used.

A fully coupled approach is adopted in solving the continuous and discrete phases of the flow. Also concerning the discrete phase, the droplet momentum, heat and mass transfer equations are solved in a fully coupled manner. For the continuous phase flow, the 3D steady RANS equations for conservation of mass, momentum and energy are solved in combination with the realizable k-ε turbulence model by Shih et al. (Shih et al., 1995) for closure. The SIMPLE algorithm is used for pressure-velocity coupling, pressure interpolation is second order and second-order discretization schemes are used for both the convection terms and the viscous terms of the equations. Lagrangian trajectory simulations are performed for the discrete phase.

Fig. 4 presents a comparison between the CFD results for the three cases, shown in Table 1, and the wind-tunnel experiments (Sureshkumar et al., 2008a). The comparison is performed for the DBT and WBT values at the nine

measurement points. The results show a good agreement, within 10% for DBT and 5% for WBT. More information on the results and sensitivity of the results to the computational parameters can be found in Ref. (Montazeri et al., 2015a).

4 CFD simulations of urban microclimate

4.1. Computational geometry

The computational domain is the combination of a circular inner subdomain, which contains the explicitly modeled buildings, i.e. with their actual shape and size, and a surrounding outer hexagonal subdomain (Fig. 5a). The diameter of the circular subdomain is 1200 meter. The edges of the hexagon are 1200 m and the height is 400 meter. The buildings inside the computational domain are represented in three levels of detail depending on their distance to the area of interest, which is the Bergpolder Zuid region. The buildings within the Bergpolder Zuid region are modeled with high resolution where geometrical details as small as 1 meter edge length are explicitly represented (Figure 5). For the buildings located in the remaining regions of Bergpolder, the resolution detail is lowered to 3-meter edge length. Finally, the remaining surrounding buildings are included with a resolution of 8-meter edge length and some of the courtyards are omitted from representation. Outside the circular subdomain, the obstacles that might affect the flow are not modeled explicitly but implicitly using appropriate roughness parameters in the standard wall functions, as recommended by best practice guidelines (Blocken, 2015). This is explained further in section 4.3.

A water spray system is employed in a courtyard where a relatively high air and surface temperature is observed from the simulations without water spray. The location of the courtyard is shown in Fig. 5c. The system consists of 15 hollow-cone spray nozzles, which are installed equidistantly at 0.5 m intervals on a single horizontal line at H = 3 m from ground level (Fig. 6).

4.2. Computational grid

The computational grid is generated by the surface-grid extrusion technique by van Hooff and Blocken (van Hooff and Blocken, 2010a). This procedure allows a large degree of control over the quality of the grid and its individual cells. It consists of only hexahedral and prismatic cells and does not contain any tetrahedral or pyramid cells. It was also used successfully in previous studies for complex building and urban configurations (e.g. (Blocken et al., 2012; Montazeri et al., 2013; Montazeri and Blocken, 2013; van Hooff and Blocken, 2010b)). The grid on the building and ground surfaces of Bergpolder Zuid and immediate surroundings is shown in Fig. 7b. It is fine in Bergpolder Zuid itself with a minimum cell size of 4.1×10^{-2} m^3 and coarser further away from this region, where the minimum cell size is 2.4×10 m^3. It is important to note that the grid has been constructed in agreement with best practice guidelines (Franke et al., 2007; Tominaga et al., 2008; Tucker and Mosquera, 2001). This includes the use of only hexahedral and prismatic cells, a minimum number of 10 cells along building edges and between neighboring buildings and wall-adjacent cell faces that are as much as possible either parallel or perpendicular to the walls. The computational domain contains a total of 6,610,456 cells.

4.3. Boundary conditions

For each of the outer faces of the hexagonal subdomain, a velocity inlet or pressure outlet boundary condition is imposed, depending on the hourly wind direction. Hourly meteorological data for the days under study are acquired from the Royal Dutch Meteorological Institute (KNMI) (Fig. 8). The meteorological data were recorded by the KNMI Rotterdam weather station, located 4 km northwest of Bergpolder Zuid, near Rotterdam airport.

At the inlets, vertical profiles for the mean wind speed (U(z) (m/s)), turbulent kinetic energy (k(z) (m^2/s^2)) and turbulence dissipation rate (ε(z) (m^2/s^3)) are imposed using the following equations (Richards and Hoxey, 1993):

$$U(z) = \frac{u^*_{ABL}}{\kappa}\, ln\left(\frac{z + z_0}{z_0}\right) \tag{3}$$

$$k(z) = \frac{u^{*2}_{ABL}}{\sqrt{C_\mu}} \tag{4}$$

$$\varepsilon(z) = \frac{u^{*3}_{ABL}}{\kappa(z + z_0)} \tag{5}$$

where z_0 (m) denotes the aerodynamic roughness length estimated using the Updated Davenport roughness classification (Fig. 2). Depending on wind direction, z_0 is defined as either 1.0 m (for the wind directions south, southeast and southwest) or 0.5 m (for the remaining wind directions) (Fig. 2). κ is the von Karman constant (= 0.41), u^* (m/s) is the friction velocity and C_μ is a model constant (= 0.09). The reference wind speed is the wind speed at 10 m height (U_{10}). In addition, a constant air temperature is imposed at the inlets. For the simulations with evaporative cooling, a fixed vapor mass fraction is imposed at the inlets. For the discrete phase, the escape boundary condition is used for the walls and the outlets.

The standard wall functions by Launder and Spalding (Launder and Spalding, 1974) are employed in combination with the equivalent sand-grain based roughness modification by Cebeci and Bradshaw (Cebeci and Bradshaw, 1977). The roughness height (k_S) and the roughness constant (C_S) are calculated based on the appropriate relationship with z_0 derived by Blocken et al. (Blocken et al., 2007) for ANSYS/Fluent:

$$k_S = \frac{9.793 z_0}{C_S} \tag{6}$$

In line with this equation, for the hexagonal subdomain, k_S = 1.39 m, C_S = 3.5 (for z_0 = 0.5 m) and k_S = 1.39 m, C_S = 7 (for z_0 = 1 m). Inside the circular subdomain, where the buildings are modeled explicitly, i.e. with their main shape, the ground plane and building walls are modeled as smooth walls with z_0 = 0 m.

A 10 m thick earth layer is modeled implicitly for the ground surface of the domain and at 10 m depth of this layer, a constant temperature of 10°C is imposed. In addition, the evapotranspiration from the ground plane is considered with a constant sink value of 80 W/m^2 during morning and afternoon (6:00-11:00 and 15:00-18:00) and 130 W/m^2 during noon (11:00-15:00). This assumption is in accordance with the observations from previous measurement studies considering heat fluxes inside dense urban areas (Grimmond and Oke, 1991; Offerle et al., 2006). The building walls are represented by brick layers with 0.4 m thickness and inside the buildings, a constant indoor air temperature of 24°C is imposed. The interior surface has a constant convective heat transfer coefficient and emissivity of 8 W/m^{2}K and 0.95, respectively. The top of the computational domain is modeled as a free slip wall and zero static pressure is imposed at the outlets.

4.4. CFD simulations of urban microclimate without evaporative cooling

The 3D Unsteady Reynolds-Averaged Navier-Stokes (URANS) equations are solved in combination with the energy equation. Closure is obtained by the realizable k-ε model. Conduction, convection and radiation are considered in the simulations, fully coupled with the wind flow. At the solid boundaries, a one-directional conduction equation is used. Natural convection is modeled with the Boussinesq approximation (Bejan, 2013) and for the radiation the P-1 radiation model is employed (ANSYS Inc., 2009). Solar load parameters such as the sun direction vector and the diffuse portion of the total radiation approaching the surface are calculated with the implemented solar calculator of ANSYS/Fluent (ANSYS Inc., 2009). The solar calculator considers a beam using the position of the sun at any time during a year and applies a radiative heat flux at the wall type boundaries that are outside the shadow. The absorption of the radiative heat by the surfaces depends on the absorptivity values, which are listed in Table 2. Pressure-velocity coupling is performed with the Semi-Implicit Method for Pressure Linked Equations (SIMPLE). For all convection and viscous terms, second-order discretization schemes are used. Unsteady simulations are performed with a time step of 900 seconds and with 60 iterations per time step, based on a time-step sensitivity analysis. For the temporal discretization, second-order implicit time integration is used.

The CFD simulations are performed for 15-19 July, 2006. To compare the simulation results with satellite imagery results, 90 sampling points are specified on the building roofs and street surfaces of the computational domain of Bergpolder Zuid to extract spatially averaged values from the CFD simulations. The sampling points are positioned on the building and ground surfaces. The selection and number of these sampling points are based on a sensitivity analysis reported in Toparlar et al. (Toparlar et al., 2015).

The results from the CFD simulations are compared with surface temperatures in Rotterdam obtained from thermal images from the NOAA-AVHRR satellite (Klok et al., 2012) taken during the same period as the CFD simulation. Although the AVHRR has a high temporal resolution which can monitor the diurnal behavior of surface temperatures, its spatial resolution is limited to 1.1 km. Therefore, the satellite results are spatially averaged surface temperatures for the districts of Rotterdam. As there is only a single value reported for each district, values for the standard deviation, minimum or maximum surface temperatures cannot be assessed. Data are available for 42 specific times within these five days. In this study, the results are compared with the satellite imagery data of the Noord region in Rotterdam that includes Bergpolder Zuid.

The comparison between the CFD simulations and the satellite imagery data is provided in Fig. 9. The simulations can repeat the diurnal variation with a fairly good agreement. The average absolute difference of surface temperatures is around 2.2 °C. The maximum difference occurs around 14:00 h on 18th of July, where CFD overestimates the measured values by 6.3°C. The exact reasons for these deviations are not clear, but they are probably caused by a combination of the following limitations, as pointed out by Toparlar et al. (Toparlar et al., 2015):

- The one-directional wall conduction approach is used at the wall boundaries. In this case, the effect of planar conduction is omitted and thus, the ground level is more prone to sudden changes in temperature, which might explain the difference in daily surface temperature variance.
- The comparison between measurement and CFD simulations is based on hourly averaged meteorological data. Hourly data might not be sufficient to produce accurate results. This is especially the case within the days where the hourly variation of wind speed and solar radiation is high.

- The influence of the thermal stratification of the atmospheric boundary layer (ABL) is not taken into consideration in the simulations. Because of this assumption, the simulated flow field might deviate from the actual one in the urban environment.
- Clouds were not included in the simulations but patch clouds might have been present locally during the measurements.
- The satellite imagery data as adopted from Klok et al. (Klok et al., 2012) presents a single value for a specific moment and for an entire district. The modeled Bergpolder Zuid region in Rotterdam constitutes only 20% of the complete Noord district. Therefore, local conditions in the complete district of Noord might not be similar to the conditions inside Bergpolder Zuid region at all times.

Contours of wind speed and air temperature at 1.75 m height (pedestrian height) at 12:00 h on July 17 are provided in Fig. 10. The temperature distribution is consistent with the wind speed distribution. In the regions with low wind speeds, air temperatures are relatively higher. This is the case for courtyards, for example, where wind speed can be significantly reduced. Fig. 11a shows the wind speed distribution at pedestrian height inside the courtyard where the spray system will be employed (Fig. 6). The velocity vector field in a vertical plane along the spray line is shown in Fig 11b. The flow in the courtyard is dominated by a recirculation zone.

4.5. CFD simulations of urban microclimate with evaporative cooling

For the simulations with evaporative cooling, the Lagrangian model for droplets and the species equations for water vapor are added.

The total injected water flow rate from the nozzles is 9.0 l/min (case 3 in Table 3). The Rosin-Rammler model (Rosin and Rammler, 1933) is used to describe the size distribution of the droplets in the CFD simulations. The smallest and largest droplet diameters to be considered in the size distribution of the Rosin-Rammler model are 10 and 60 μm, respectively. The mean of the Rosin-Rammler distribution, $\overline{D}$ and the spread parameter, n are 20 μm and 3.5, respectively. The injected water temperature is 25 °C.

The droplets are injected into the domain and trajectory calculations are performed at 12:00 h on July 17. The 3D steady RANS equations are solved for conservation of momentum, heat and mass. Note that all boundary conditions (i.e. meteorological conditions) are fixed, identical to those at 12:00 h. Inlet mean wind speed is 3 m/s, wind direction is 80°, inlet air temperature is 29.7 °C and inlet air relative humidity is 33%. In this case, the vapor mass fraction at the inlet is about 8.5×10^{-3}. The droplets are treated in a steady-state fashion. The discrete phase interacts with the continuous phase in a fully coupled manner and the discrete phase model source terms are updated after each continuous phase iteration. The correlation by Morsi and Alexander (Morsi and Alexander, 1972) is used for the droplet drag coefficients. To solve the equations of motion for the droplets, the Automated Tracking Scheme Selection is adopted to be able to switch between higher order and lower order tracking schemes. This mechanism can improve the accuracy and stability of the simulations (ANSYS Inc., 2009). In this study, trapezoidal and implicit schemes are used for higher-order and lower-order schemes, respectively.

The impact of evaporative cooling by a water spray system on human heat stress depends on the complex interaction between different climatic variables (Saneinejad et al., 2012) and spray characteristics (Farnham et al., 2015; Montazeri et al., 2015b). It can be assessed by the Universal Thermal Climate Index (UTCI) (Fiala et al., 2012; Jendritzky et al., 2012) which is a heat stress/thermal comfort indicator for outdoor and semi-enclosed environments. It is an equivalent temperature, derived based on the Fiala multi-node model (Fiala et al., 2001, 1999), which reflects the human physiological reaction to meteorological parameters including air temperature and humidity, wind speed and mean radiant temperature, T_{mrt} (Bröde et al., 2012). In this study, the first three quantities are a direct output of the CFD simulations. A constant T_{mrt} value is assumed in the courtyard before and after spraying water, T_{mrt} = 45 °C, in accordance with the results of previous simulation studies for the city of Rotterdam (Dai and Schnabel, 2013) and on-site measurements for similar urban areas (e.g. (Tan et al., 2013)). The UTCI values can be categorized into ten levels of thermal stress ranging from “extreme cold stress” to “extreme heat stress” (Table 4 (Bröde et al., 2012)).

To evaluate the cooling performance of the spray system inside the courtyard (Figs. 5c and 6), the results are compared for two cases, with and without spray system. Figs. 12a and c show the distributions of air temperature and vapor mass fraction across a horizontal plane (1.75 m from ground height) for the case without spray system. The results are provided for 12:00 h on July 17. A relatively uniform air temperature distribution can be observed at this height, where the wind speed is relatively low (0.5 – 1.5 m/s) (Fig. 11a). Note that the air temperature is 2-4 °C higher than the inlet air temperature (meteorological data) at the same time (i.e. 30 °C). In this case, the average UTCI at this height is almost constant (34.4 °C), which indicates the “strong heat stress” level (Table 4).

Figs. 12b and d present the results when the spray system is in operation. In this case, the injected water flow rate is $\dot{m}_w$ = 9.0 l/min and the system is installed at H = 3 m. It can be seen that the maximum temperature reduction (about 7 °C) occurs underneath the spray system in the middle of the spray line. From these figures, the relatively symmetric air temperature and humidity (vapor mass fraction) distributions on both sides of the spray line can be clearly observed. However, a clockwise circulation flow, when viewed from the positive y-axis (Fig. 11b), in the courtyard leads to the advection of the cool air and moisture to the right-hand side of the courtyard. The spray system retains some cooling

effect away from the nozzles. For example, the temperature reduction is more than 2 °C up to a distance of 8 m away from the spray line.

5. CFD simulations for parametric analysis

5.1. Impact of water flow rate

Fig. 13 shows the distributions of air temperature and vapor mass fraction at pedestrian height for $\dot{m}_w$ = 2.25, 4.50, 9.0 l/min (cases 1 – 3 in Table 3). The height of the spray system is identical (H = 3 m) for the three cases. The maximum temperature reduction and vapor mass fraction increase are achieved at the same position underneath the spray line. By increasing $\dot{m}_w$ from 2.25 to 9.0 l/min, the air temperature reduces across the plane monotonically, while the vapor mass fraction increases.

Fig. 14 presents the profiles of the air temperature, vapor mass fraction and UTCI variation along a line at pedestrian height in the middle of the courtyard for the different values of $\dot{m}_w$. The maximum air temperature reduction increases from about 1 to 7 °C as $\dot{m}_w$ increases from 2.25 to 9.0 l/min. In addition, for higher values of $\dot{m}_w$, the cooling effect extends further away from the spray line. For example, 8 m away from the spray line the temperature reduction is more than 2 and 1 °C for the cases with $\dot{m}_w$ = 9.0 and 4.45 l/min, while no cooling effect is observed for the case with $\dot{m}_w$ = 2.25 l/min. The UTCI reduction, as an indicator for heat stress reduction, is shown in Fig. 14c. The maximum UTCI reduction increases from about 1 °C for $\dot{m}_w$ = 2.25 l/min to about 5 °C for $\dot{m}_w$ = 9.0 l/min. For the case with the highest injected water flow rate, this reduction leads to an improvement from strong heat stress (without spray system) to moderate heat stress up to a distance of 5 m from the spray line (Table 4).

5.2. Impact of height of the spray system

The height of a water spray system can affect the cooling performance of the system, but also wetting of people and surfaces (Farnham et al., 2011). In this subsection, results for H = 3, 4 and 5 m (cases 3 – 5 in Table 3) are presented. The distributions of air temperature and vapor mass fraction at the horizontal plane at pedestrian height are shown in Fig. 15. By increasing H, the maximum cooling effect of the spray system on the target zone (pedestrian height) decreases monotonically. Note that complete evaporation takes place for the three cases.

Fig. 16 indicates the profiles of the air temperature, vapor mass fraction and UTCI variations along a horizontal line in the middle of the domain (pedestrian height) for different values of H. The maximum air temperature reduction decreases by about 2 °C as H increases from 3 m to 5 m. In this case, the maximum UTCI reduction also decreases from about 5 to 3 °C, respectively.

6. Discussion

This paper presents CFD simulations on a high-resolution grid to assess the cooling potential of a water spray system with hollow-cone nozzles for a courtyard in an actual urban area. However, the accuracy and reliability of CFD simulations are of concern and solution verification and validation studies are imperative (Blocken, 2014). This requires high-resolution high-quality full-scale or reduced-scale measurements. However, such measurement data for water spray systems in an actual urban area is lacking. Therefore, so-called sub-configuration validation has been used in the present research. Sub-configuration validation refers to performing validation for simpler generic building configurations that represent sub-configurations of the more complex urban configuration. For these generic configurations, wind-tunnel measurements are generally available in the literature. The confidence extracted from this validation study can be used to support the application of CFD with similar computational parameters for the more complex urban configuration.

In the present study, a water spray system is employed in a courtyard with a relatively low wind speed (1.2 m/s) and high air temperature (32-34 °C). Research shows that higher values of air speed relative to the water droplets can improve the cooling performance of water spray systems (Montazeri et al., 2015b). On the other hand, in areas with a relatively high wind speed, water droplets might be blown sideways, which could lead to a lower cooling effect in the intended target zone.

This study has been performed in a relatively low atmospheric humidity (RH = 33%). It should be noted that in the Netherlands the warmest period of the year usually coincides with relatively low values of relative humidity. During the major European heat wave in 2006, for example, the relative humidity during daytime (when most cooling for outdoor environments is needed) was less than 45% in the Dutch city of Rotterdam, while the air temperature was higher than 30 °C. Further research is needed to quantify the cooling performance of water spray systems in more humid climate conditions.

In this study, the cooling performance of a water spray system consisting of several spray nozzles is evaluated for a public space (building and street scale). Further research needs to be performed to assess the performance of such systems at the building scale, in which a spray system can be used in combination with a fan.

During the design of similar evaporative cooling systems, special attention needs to be paid to the quality of air in zones under the influence of the system. For instance, the risk of bacterial growth in humid environments is a well-known issue. This can be done, for example, using on-site measurements. In addition, using clean water is essential to ensure it

does not affect the quality of the air. In some cases, the supply water is required to be chlorinated (Farnham et al., 2015). Further research needs to be performed to investigate the importance of water quality in mist spraying systems.

7. Conclusions

This paper presents high-resolution Computational Fluid Dynamics (CFD) simulations based on the 3D unsteady Reynolds-Averaged Navier-Stokes equations to assess the cooling potential and heat stress reduction by a water spray system with 15 hollow-cone nozzles. The system is numerically implemented in the Bergpolder Zuid region of the Dutch city of Rotterdam and operated at a specific moment during the heat wave period of July 2006. To simulate the two-phase flow, the Lagrangian-Eulerian approach is implemented. The CFD simulations are validated based on wind-tunnel measurements of an evaporative cooling process and on field measurements of surface temperatures during the heat wave period (without water spraying). The Universal Thermal Climate Index (UTCI) is used to assess the heat stress improvement due to evaporative cooling.

The results show that for given values of injected water flow rate ($\dot{m}_w$ = 9.0 l/min) and height of the spray system (H = 3 m), a maximum temperature reduction and UTCI reduction of about 7 and 5 °C are achieved at pedestrian height (1.75 m) in the courtyard. In addition, a thermal comfort improvement from strong heat stress (without spray system) to moderate heat stress up to a distance of 5 m from the spray line is observed.

From the research presented in this paper it can be concluded that CFD simulations can be used to provide accurate and reliable data on urban microclimate for the evaluation of heat stress and of evaporative cooling as a measure to reduce heat stress in urban areas. As the need for climate adaptation increases, it will become important for landscape architects and urban planners to integrate climate change adaptation measures in both new designs and redesigns of landscapes and urban areas. This paper has demonstrated that evaporative cooling by water spray systems can be an effective adaptation measure. Landscape architects and urban planners are encouraged to consider aesthetically acceptable ways of integrating water spray systems in new designs or redesigns wherever deemed necessary and appropriate.

Acknowledgments

Hamid Montazeri is currently a postdoctoral fellow of the Research Foundation – Flanders (FWO) and is grateful for its financial support (project FWO 12M5316N).

References

Akbari, H., Bretz, S., Kum, D., Hanford, J., 1997. Peak power and cooling energy savings of high-albedo roofs. Energy Build. 25, 117–126.

Albers, R.A.W., Bosch, P.R., Blocken, B., Van Den Dobbelsteen, A., Van Hove, L.W.A., Spit, T.J.M., van de Ven, F., van Hooff, T., Rovers, V., 2015. Overview of challenges and achievements in the Climate Adaptation of Cities and in the Climate Proof Cities program. Build. Environ. 83, 1–10.

Allegrini, J., Dorer, V., Carmeliet, J., 2012. Influence of the urban microclimate in street canyons on the energy demand for space cooling and heating of buildings. Energy Build. 55, 823–832.

ANSYS Inc., 2009. ANSYS Inc. ANSYS Fluent 12.0 Theory Guide. USA: Lebanon.

Ashgriz, N., 2011. Handbook of atomization and sprays: theory and applications. Springer.

Bejan, A., 2013. Convection heat transfer. John wiley & sons.

Blocken, B., 2015. Computational Fluid Dynamics for urban physics: Importance, scales, possibilities, limitations and ten tips and tricks towards accurate and reliable simulations. Build. Environ. 91, 219–245.

Blocken, B., 2014. 50 years of Computational Wind Engineering: Past, present and future. J. Wind Eng. Ind. Aerodyn. 129, 69–102.

Blocken, B., Carmeliet, J., 2004. A review of wind-driven rain research in building science. J. Wind Eng. Ind. Aerodyn. 92, 1079–1130.

Blocken, B., Janssen, W.D., van Hooff, T., 2012. CFD simulation for pedestrian wind comfort and wind safety in urban areas: General decision framework and case study for the Eindhoven University campus. Environ. Model. Softw. 30, 15–34.

Blocken, B., Stathopoulos, T., Carmeliet, J., 2007. CFD simulation of the atmospheric boundary layer: wall function problems. Atmos. Environ. 41, 238–252.

Bröde, P., Fiala, D., Błażejczyk, K., Holmér, I., Jendritzky, G., Kampmann, B., Tinz, B., Havenith, G., 2012. Deriving the operational procedure for the Universal Thermal Climate Index (UTCI). Int. J. Biometeorol. 56, 481–494.

Calautit, J.K., Hughes, B.R., Chaudhry, H.N., Ghani, S.A., 2013. CFD analysis of a heat transfer device integrated wind tower system for hot and dry climate. Appl. Energy 112, 576–591.

Casey, M., Wintergerste, T., 2000. Best Practice Guidelines: ERCOFTAC Special Interest Group on“ Quality and Trust in Industrial CFD.” ERCOFTAC.

Cebeci, T., Bradshaw, P., 1977. Momentum transfer in boundary layers. Wash. DC Hemisphere Publ. Corp N. Y. McGraw-Hill Book Co 1977 407 P 1.

Dai, Q., Schnabel, M.A., 2013. Relationship between Mean Radiant Temperature and Building Type for Pedestrians in Rotterdam, in: Zhang, J., Sun, C. (Eds.), Global Design and Local Materialization: 15th International

Conference, CAAD Futures 2013, Shanghai, China, July 3-5, 2013. Proceedings. Springer Berlin Heidelberg, Berlin, Heidelberg, pp. 306–314.
Farnham, C., Emura, K., Mizuno, T., 2015. Evaluation of cooling effects: outdoor water mist fan. Build. Res. Inf. 43, 334–345.
Farnham, C., Nakao, M., Nishioka, M., Nabeshima, M., Mizuno, T., 2011. Study of mist-cooling for semi-enclosed spaces in Osaka, Japan. Procedia Environ. Sci. 4, 228–238.
Fiala, D., Havenith, G., Bröde, P., Kampmann, B., Jendritzky, G., 2012. UTCI-Fiala multi-node model of human heat transfer and temperature regulation. Int. J. Biometeorol. 56, 429–441.
Fiala, D., Lomas, K.J., Stohrer, M., 2001. Computer prediction of human thermoregulatory and temperature responses to a wide range of environmental conditions. Int. J. Biometeorol. 45, 143–159.
Fiala, D., Lomas, K.J., Stohrer, M., 1999. A computer model of human thermoregulation for a wide range of environmental conditions: the passive system. J. Appl. Physiol. 87, 1957–1972.
Fischer, P.H., Brunekreef, B., Lebret, E., 2004. Air pollution related deaths during the 2003 heat wave in the Netherlands. Atmos. Environ. 38, 1083–1085.
Franke, J., Hellsten, A., Schlünzen, H., Carissimo, B., 2007. Best practice guideline for the CFD simulation of flows in the urban environment. COST action 732: quality assurance and improvement of microscale meteorological models.
Grimmond, C.S.B., Oke, T.R., 1991. An evapotranspiration-interception model for urban areas. Water Resources Research 27, 1739–1755.
Gromke, C., Blocken, B., Janssen, W., Merema, B., van Hooff, T., Timmermans, H., 2015. CFD analysis of transpirational cooling by vegetation: Case study for specific meteorological conditions during a heat wave in Arnhem, Netherlands. Build. Environ. 83, 11–26.
Haines, A., Kovats, R.S., Campbell-Lendrum, D., Corvalán, C., 2006. Climate change and human health: Impacts, vulnerability and public health. Public Health 120, 585–596.
Heusinkveld, B.G., Steeneveld, G.J., Hove, L.W.A., Jacobs, C.M.J., Holtslag, A.A.M., 2013. Spatial variability of the Rotterdam urban heat island as influenced by urban land use. J. Geophys. Res. Atmospheres.
Huang, C., Ye, D., Zhao, H., Liang, T., Lin, Z., Yin, H., Yang, Y., 2011. The research and application of spray cooling technology in Shanghai Expo. Appl. Therm. Eng. 31, 3726–3735.
Isaac, M., Van Vuuren, D.P., 2009. Modeling global residential sector energy demand for heating and air conditioning in the context of climate change. Energy Policy 37, 507–521.
Jendritzky, G., de Dear, R., Havenith, G., 2012. UTCI—Why another thermal index? Int. J. Biometeorol. 56, 421–428.
Kang, D., Strand, R.K., 2013. Modeling of simultaneous heat and mass transfer within passive down-draft evaporative cooling (PDEC) towers with spray in FLUENT. Energy Build. 62, 196–209.
Klok, L., Zwart, S., Verhagen, H., Mauri, E., 2012. The surface heat island of Rotterdam and its relationship with urban surface characteristics. Resour. Conserv. Recycl. 64, 23–29.
Kovats, R.S., Hajat, S., 2008. Heat stress and public health: a critical review. Annu Rev Public Health 29, 41–55.
Launder, B.E., Spalding, D.B., 1974. The numerical computation of turbulent flows. Comput. Methods Appl. Mech. Eng. 3, 269–289.
Lefebvre, A.H., 1989. Properties of sprays. Part. Part. Syst. Charact. 6, 176–186.
Loonen, R., Trčka, M., Cóstola, D., Hensen, J.L.M., 2013. Climate adaptive building shells: State-of-the-art and future challenges. Renew. Sustain. Energy Rev. 25, 483–493.
Mirzaei, P.A., Haghighat, F., 2010. Approaches to study urban heat island–abilities and limitations. Build. Environ. 45, 2192–2201.
Mochida, A., Lun, I.Y., 2008. Prediction of wind environment and thermal comfort at pedestrian level in urban area. J. Wind Eng. Ind. Aerodyn. 96, 1498–1527.
Montazeri, H., 2011. Experimental and numerical study on natural ventilation performance of various multi-opening wind catchers. Build. Environ. 46, 370–378.
Montazeri, H., Azizian, R., 2009. Experimental study on natural ventilation performance of a two-sided wind catcher. Proc. Inst. Mech. Eng. Part J. Power Energy 223, 387–400.
Montazeri, H., Blocken, B., 2013. CFD simulation of wind-induced pressure coefficients on buildings with and without balconies: validation and sensitivity analysis. Build. Environ. 60, 137–149.
Montazeri, H., Blocken, B., Hensen, J.L.M., 2015a. Evaporative cooling by water spray systems: CFD simulation, experimental validation and sensitivity analysis. Build. Environ. 83, 129–141.
Montazeri, H., Blocken, B., Hensen, J.L.M., 2015b. CFD analysis of the impact of physical parameters on evaporative cooling by a mist spray system. Appl. Therm. Eng. 75, 608–622.
Montazeri, H., Blocken, B., Janssen, W.D., van Hooff, T., 2013. CFD evaluation of new second-skin facade concept for wind comfort on building balconies: Case study for the Park Tower in Antwerp. Build. Environ. 68, 179–192.
Montazeri, H., Montazeri, F., Azizian, R., Mostafavi, S., 2010. Two-sided wind catcher performance evaluation using experimental, numerical and analytical modeling. Renew. Energy 35, 1424–1435.
Morsi, S.A., Alexander, A.J., 1972. An investigation of particle trajectories in two-phase flow systems. J Fluid Mech 55, 193–208.

Murakami, S., 1997. Current status and future trends in computational wind engineering. J. Wind Eng. Ind. Aerodyn. 67-68, 3–34.
Murakami, S., Ooka, R., Mochida, A., Yoshida, S., Kim, S., 1999. CFD analysis of wind climate from human scale to urban scale. J. Wind Eng. Ind. Aerodyn. 81, 57–81.
Nishimura, N., Nomura, T., Iyota, H., Kimoto, S., 1998. Novel water facilities for creation of comfortable urban micrometeorology. Sol. Energy 64, 197–207.
Offerle, B., Grimmond, C.S.B., Fortuniak, K., Klysik, K., Oke, T.R., 2006. Temporal variations in heat fluxes over a central European city centre. Theor. Appl. Climatol. 84, 103–115.
Oke, T.R., 1982. The energetic basis of the urban heat island. Q. J. R. Meteorol. Soc. 108, 1–24.
Parry, M.L., Canziani, O.F., Palutikof, J.P., van der Linden, P.J., Hanson, C.E., 2007. Climate Change 2007: Impacts, Adaptation and Vulnerability: Working Group II Contribution to the Fourth Assessment Report of the IPCC Intergovernmental Panel on Climate Change. Cambridge University Press.
Pearlmutter, D., Erell, E., Etzion, Y., Meir, I.A., Di, H., 1996. Refining the use of evaporation in an experimental down-draft cool tower. Energy Build. 23, 191–197.
Ramponi, R., Blocken, B., 2012. CFD simulation of cross-ventilation for a generic isolated building: impact of computational parameters. Build. Environ. 53, 34–48.
Richards, P.J., Hoxey, R.P., 1993. Appropriate boundary conditions for computational wind engineering models using the k-ϵ turbulence model. J. Wind Eng. Ind. Aerodyn. 46, 145–153.
Rizwan, A.M., Dennis, L.Y., Chunho, L.I.U., 2008. A review on the generation, determination and mitigation of Urban Heat Island. J. Environ. Sci. 20, 120–128.
Robine, J.-M., Cheung, S.L.K., Le Roy, S., Van Oyen, H., Griffiths, C., Michel, J.-P., Herrmann, F.R., 2008. Death toll exceeded 70,000 in Europe during the summer of 2003. C. R. Biol. 331, 171–178.
Rosenfeld, A.H., Akbari, H., Bretz, S., Fishman, B.L., Kurn, D.M., Sailor, D., Taha, H., 1995. Mitigation of urban heat islands: materials, utility programs, updates. Energy Build. 22, 255–265.
Rosin, P., Rammler, E., 1933. The Laws Governing the Fineness of Powdered Coal. J. Inst. Fuel 31, 29–36.
Saneinejad, S., Moonen, P., Defraeye, T., Derome, D., Carmeliet, J., 2012. Coupled CFD, radiation and porous media transport model for evaluating evaporative cooling in an urban environment. J. Wind Eng. Ind. Aerodyn. 104, 455–463.
Shih, T.-H., Liou, W.W., Shabbir, A., Yang, Z., Zhu, J., 1995. A new k-ϵ eddy viscosity model for high reynolds number turbulent flows. Comput. Fluids 24, 227–238.
Stathopoulos, T., 2002. The numerical wind tunnel for industrial aerodynamics: Real or virtual in the new millennium? Wind Struct. 5, 193–208.
Stathopoulos, T., 1997. Computational wind engineering: Past achievements and future challenges. J. Wind Eng. Ind. Aerodyn. 67, 509–532.
Stott, P.A., Stone, D.A., Allen, M.R., 2004. Human contribution to the European heatwave of 2003. Nature 432, 610–614.
Strahler, A.N., Strahler, A.H., 1984. Elements of physical geography. John Wiley & Sons.
Sureshkumar, R., Kale, S.R., Dhar, P.L., 2008a. Heat and mass transfer processes between a water spray and ambient air–I. Experimental data. Appl. Therm. Eng. 28, 349–360.
Sureshkumar, R., Kale, S.R., Dhar, P.L., 2008b. Heat and mass transfer processes between a water spray and ambient air–II. Simulations. Appl. Therm. Eng. 28, 361–371.
Takahashi, R., Asakura, A., Koike, K., Himeno, S., Fujita, S., 2010. Using snow melting pipes to verify water sprinkling's effect over a wide area. Sustain. Tech. Strateg. Urban Water Manag.
Taleghani, M., Tenpierik, M., van den Dobbelsteen, A., 2014. Energy performance and thermal comfort of courtyard/atrium dwellings in the Netherlands in the light of climate change. Renew. Energy 63, 486–497.
Tominaga, Y., Mochida, A., Yoshie, R., Kataoka, H., Nozu, T., Yoshikawa, M., Shirasawa, T., 2008. AIJ guidelines for practical applications of CFD to pedestrian wind environment around buildings. J. Wind Eng. Ind. Aerodyn. 96, 1749–1761.
Tominaga, Y., Stathopoulos, T., 2013. CFD simulation of near-field pollutant dispersion in the urban environment: A review of current modeling techniques. Atmos. Environ. 79, 716–730.
Toparlar, Y., Blocken, B., Vos, P., van Heijst, G.J.F., Janssen, W.D., van Hooff, T., Montazeri, H., Timmermans, H.J.P., 2015. CFD simulation and validation of urban microclimate: A case study for Bergpolder Zuid, Rotterdam. Build. Environ. 83, 79–90.
Tucker, P., Mosquera, A., 2001. NAFEMS Introduction to Grid and Mesh Generation for CFD. NAFEMS CFD Working Group, R0079, 56pp.
van Hooff, T., Blocken, B., 2010a. Coupled urban wind flow and indoor natural ventilation modelling on a high-resolution grid: A case study for the Amsterdam ArenA stadium. Environ. Model. Softw. 25, 51–65.
van Hooff, T., Blocken, B., 2010b. On the effect of wind direction and urban surroundings on natural ventilation of a large semi-enclosed stadium. Comput. Fluids 39, 1146–1155.
van Hooff, T., Blocken, B., Hensen, J.L.M., Timmermans, H.J.P., 2014. On the predicted effectiveness of climate adaptation measures for residential buildings. Build. Environ. 82, 300–316.

van Hooff, T., Blocken, B., Timmermans, H.J.P., Hensen, J.L.M., 2016. Analysis of the predicted effect of passive climate adaptation measures on energy demand for cooling and heating in a residential building. Energy 94, 811 – 820.
Wieringa, J., 1992. Updating the Davenport roughness classification. J. Wind Eng. Ind. Aerodyn. 41, 357–368.

Figures

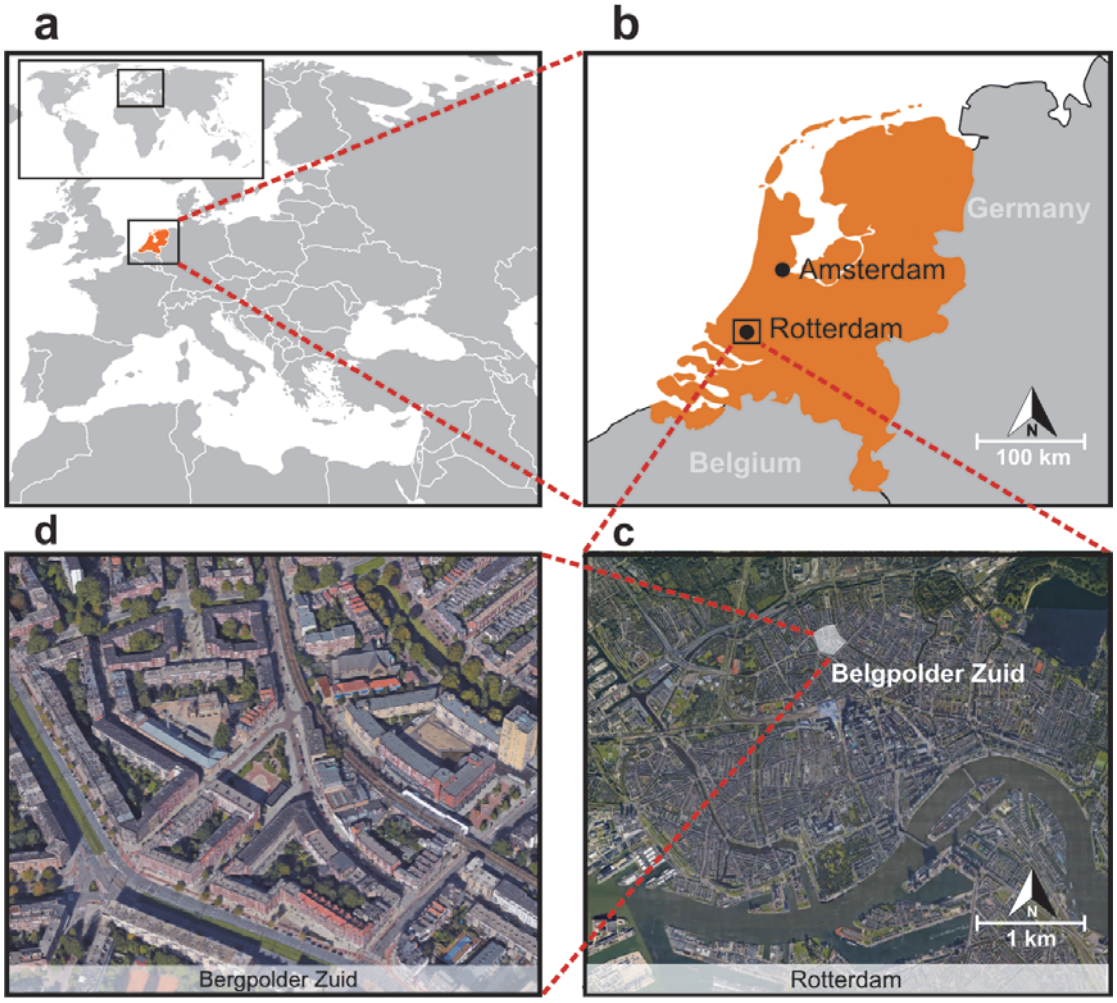

Fig. 1 Case study area at various spatial scales. (a) The Netherlands. (b) The city of Rotterdam. (c) Bergpolder Zuid district. (d) Aerial view of the district. (Figures modified from Google Maps).

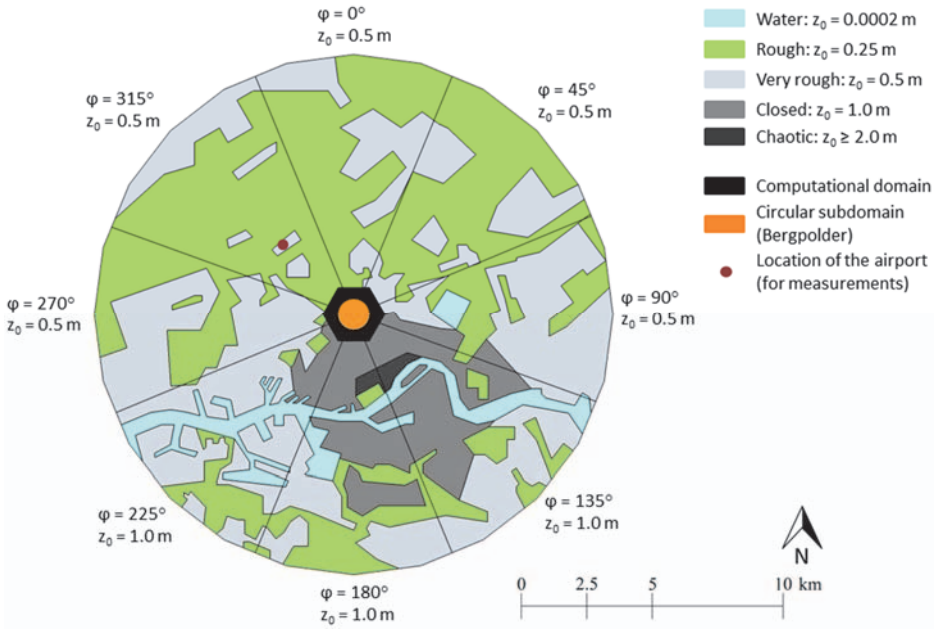

Fig. 2 Terrain surrounding the modeled urban area with a radius of 10 km. The estimated aerodynamic roughness length (z_0) is shown for different upstream fetches. The computational domain used in this study is represented by the black hexagon in the middle.

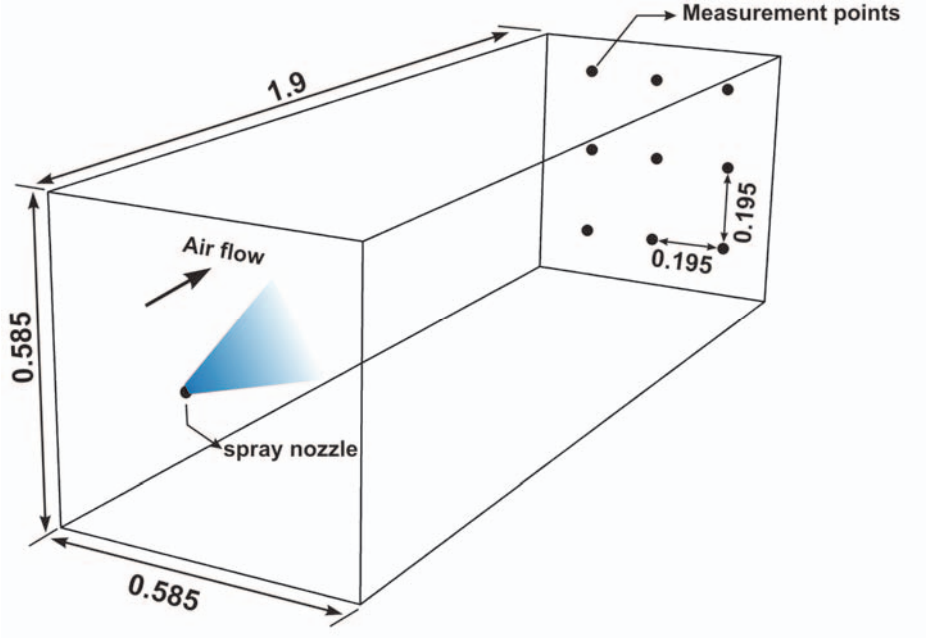

Fig. 3 Evaporative cooling validation study: computational domain including spray nozzle and measurement points (dimensions in meter).

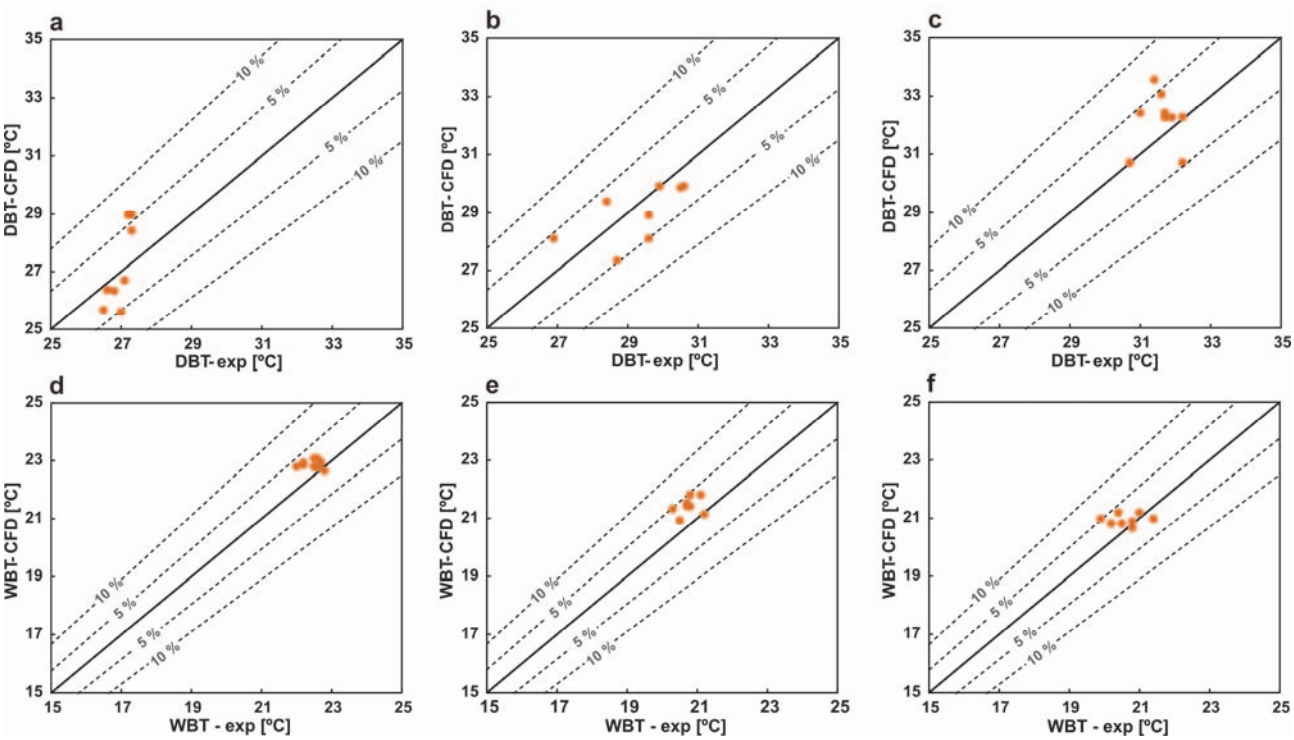

Fig. 4 Comparison of calculated (CFD) and measured (Sureshkumar et al., 2008a) (a-c) DBT and (d-f) WBT for case 1, 2 and 3, respectively.

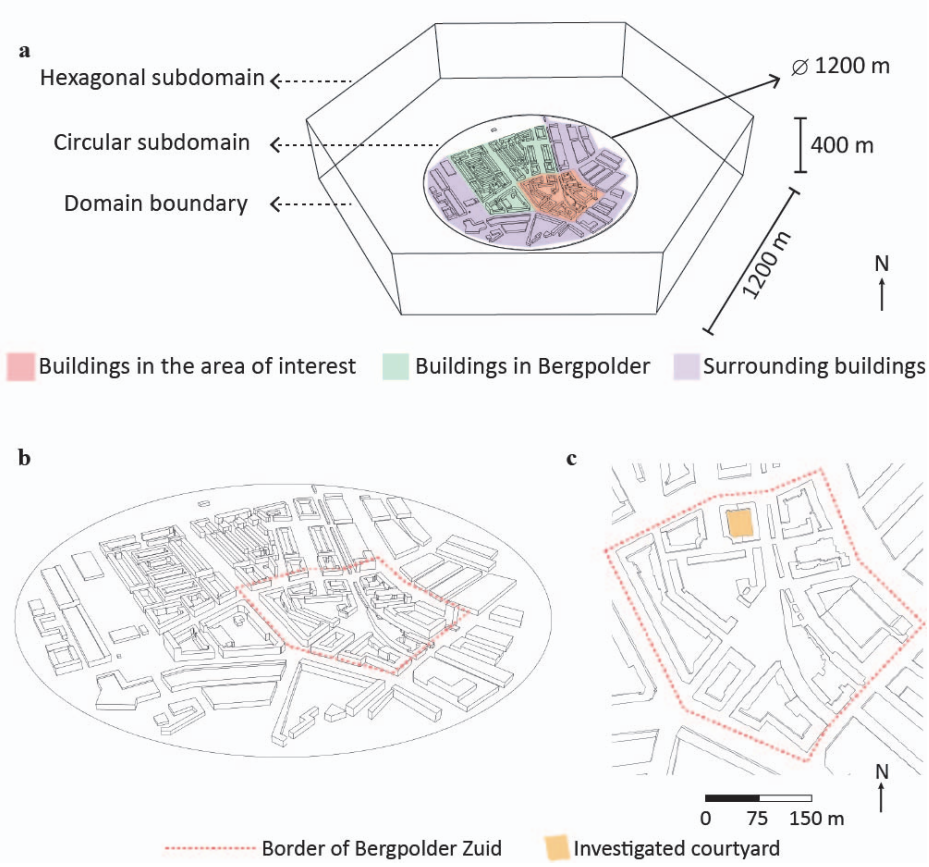

Fig. 5 (a) Computational domain and geometry. Different colors represent different categories of buildings in terms of detail in modeling; (b) Building and street surfaces as in the computational domain; (c) top view of the Bergpolder Zuid region.

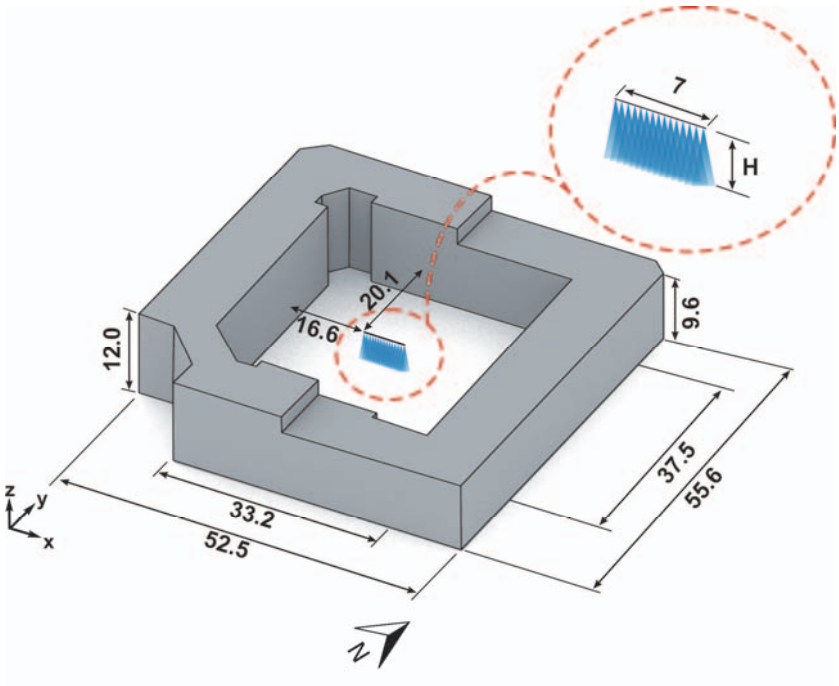

Fig. 6 Perspective view and section of the courtyard along with the water spray system (dimensions in meter).

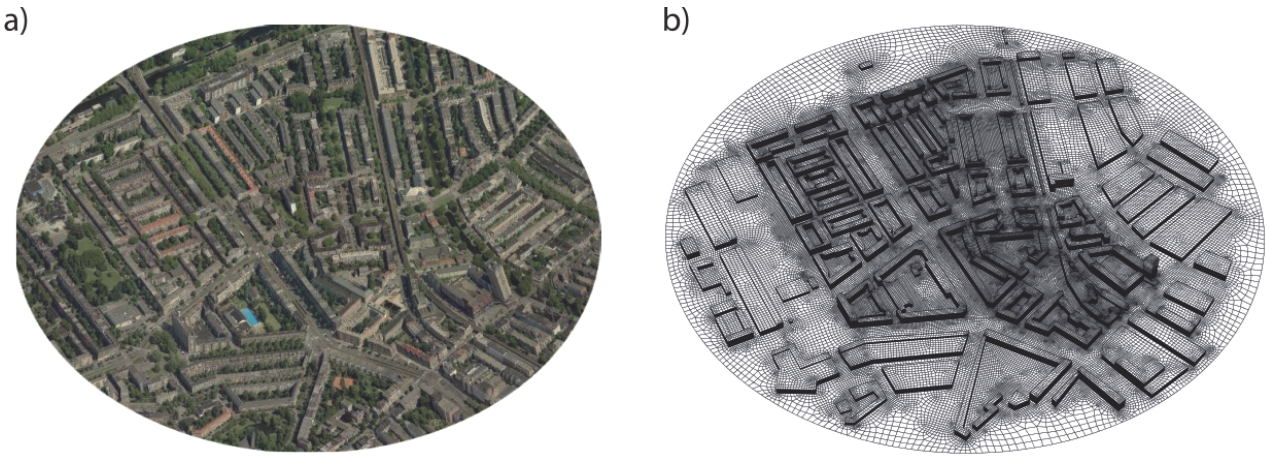

Fig. 7 (a) Aerial view of the Bergpolder Zuid region (Source: Google Maps). (b) Computational grid on the building surfaces and on part of the ground surface. The intensity of black lines indicates areas with a higher grid resolution (total number of cells: 6,610,456).

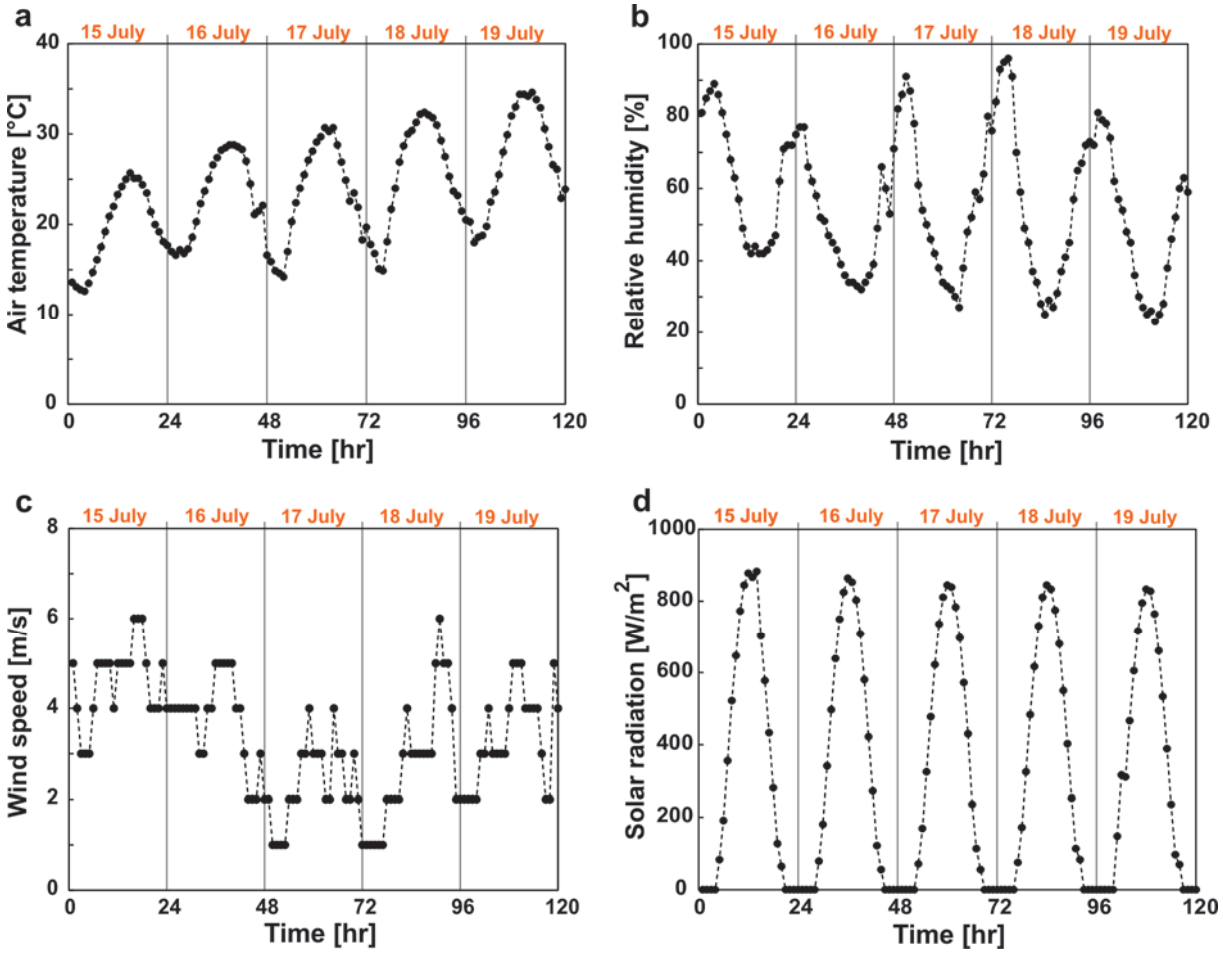

Fig. 8 Meteorological data (of KNMI-Rotterdam weather station) during 15, 16, 17, 18 and 19 July 2006. Acquired from the hourly dataset of KNMI for: (a) air temperature; (b) relative humidity; (c) wind speed and (d) solar radiation.

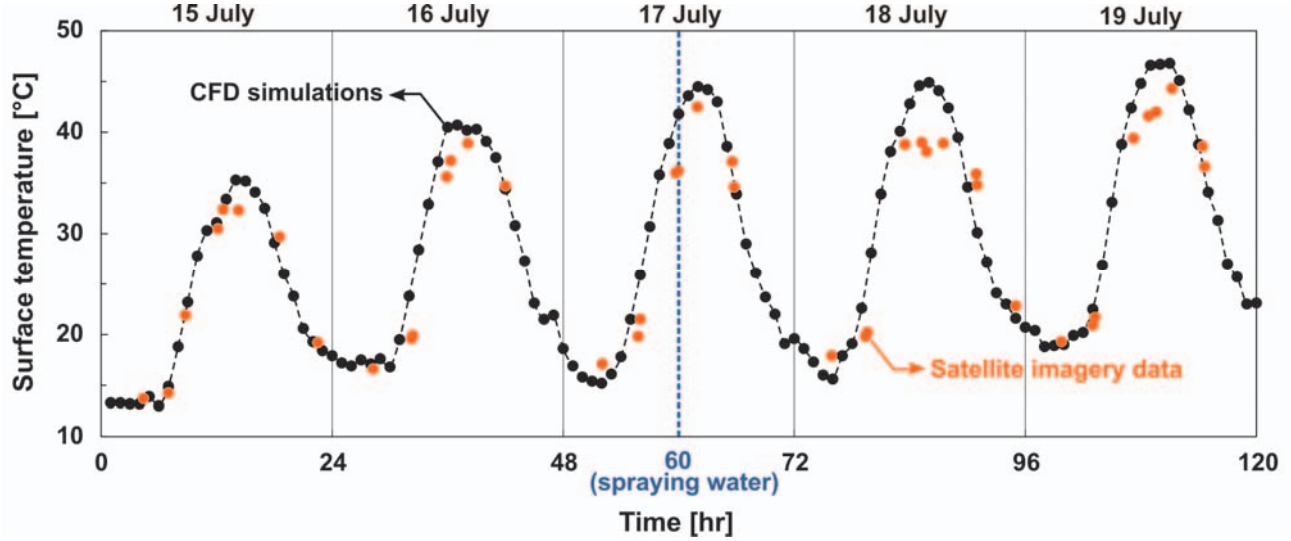

Fig. 9 Urban microclimate validation study: Comparison of average surface temperatures for five consecutive days from CFD simulation and satellite imagery.

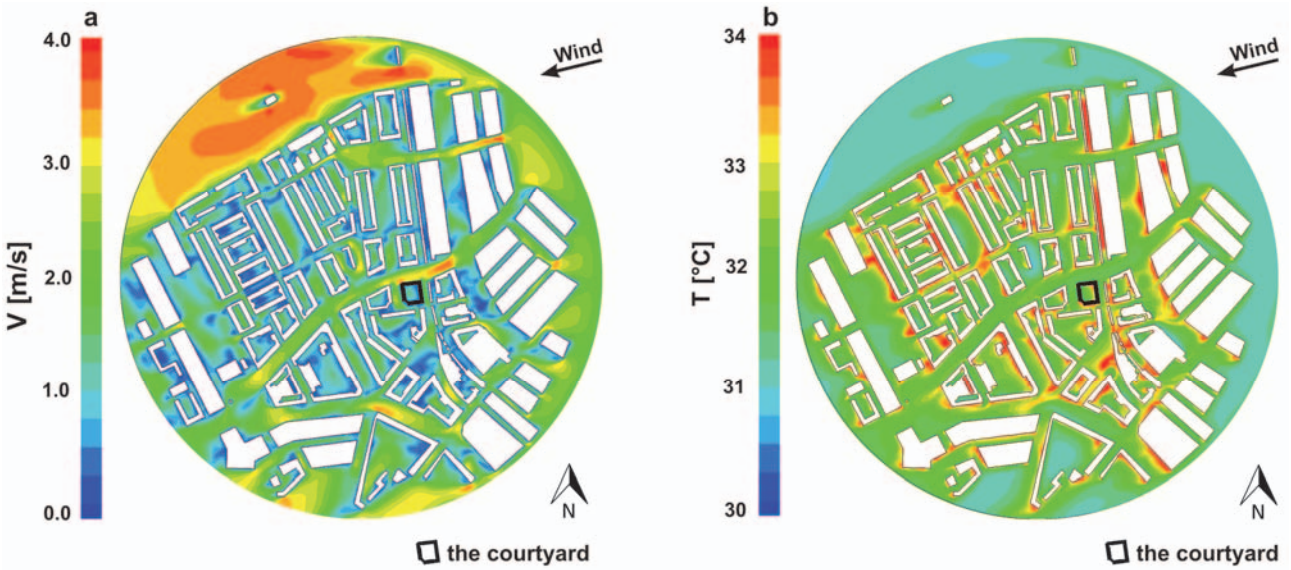

Fig. 10 (a) Air velocity and (b) air temperature distribution at pedestrian height (1.75 m) for July 17, 2006: 12:00 h.

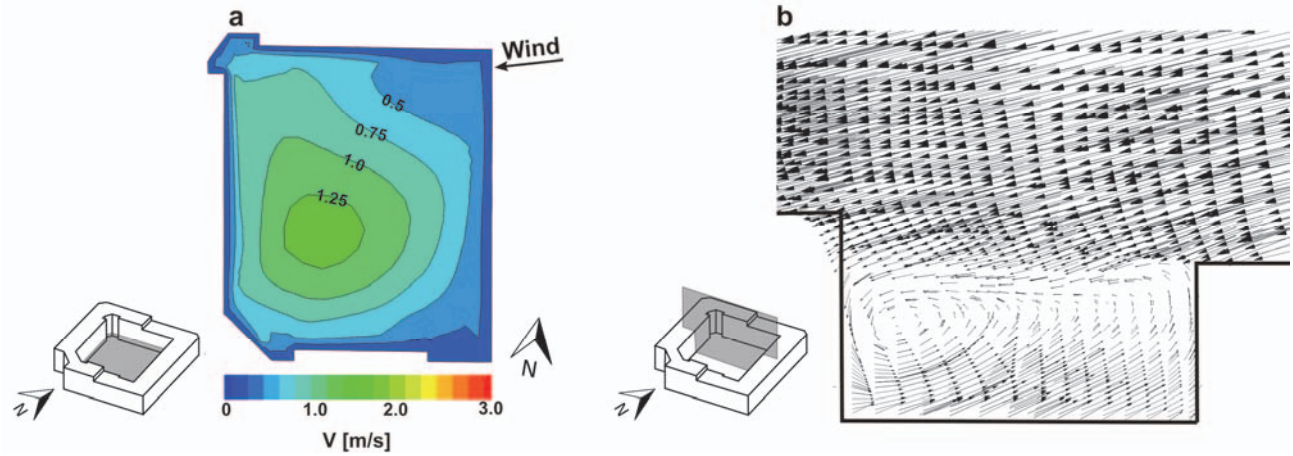

Fig. 11 (a) Wind speed distribution in a horizontal plane at a height of 1.75 m above ground level, and (b) velocity vector field in a vertical plane in the courtyard for the case without spray.

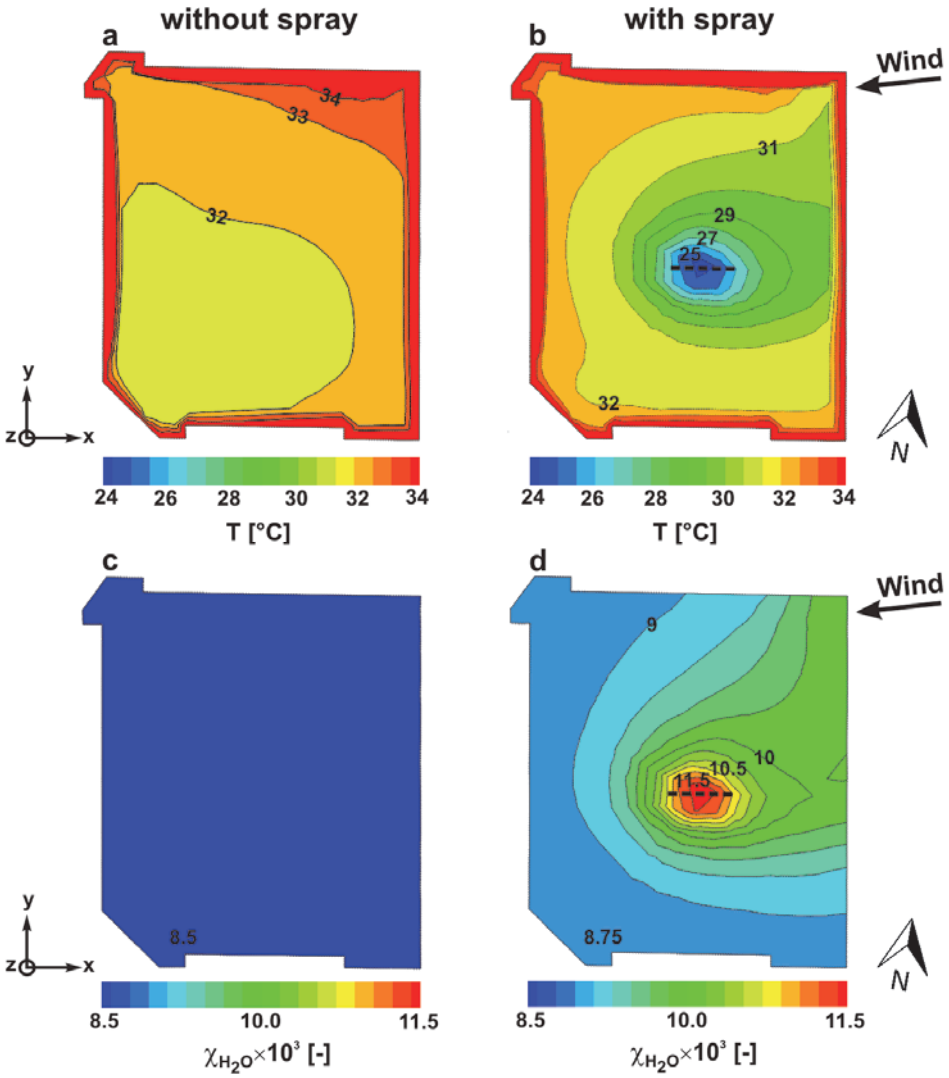

Fig. 12 Air temperature distribution in a horizontal plane at a height of 1.75 m above ground level for the case (a) without and (b) with spray (July 17, 2006: 12.00 h). (c,d) Same for vapor mass fraction. The dashed line indicates the spray line.

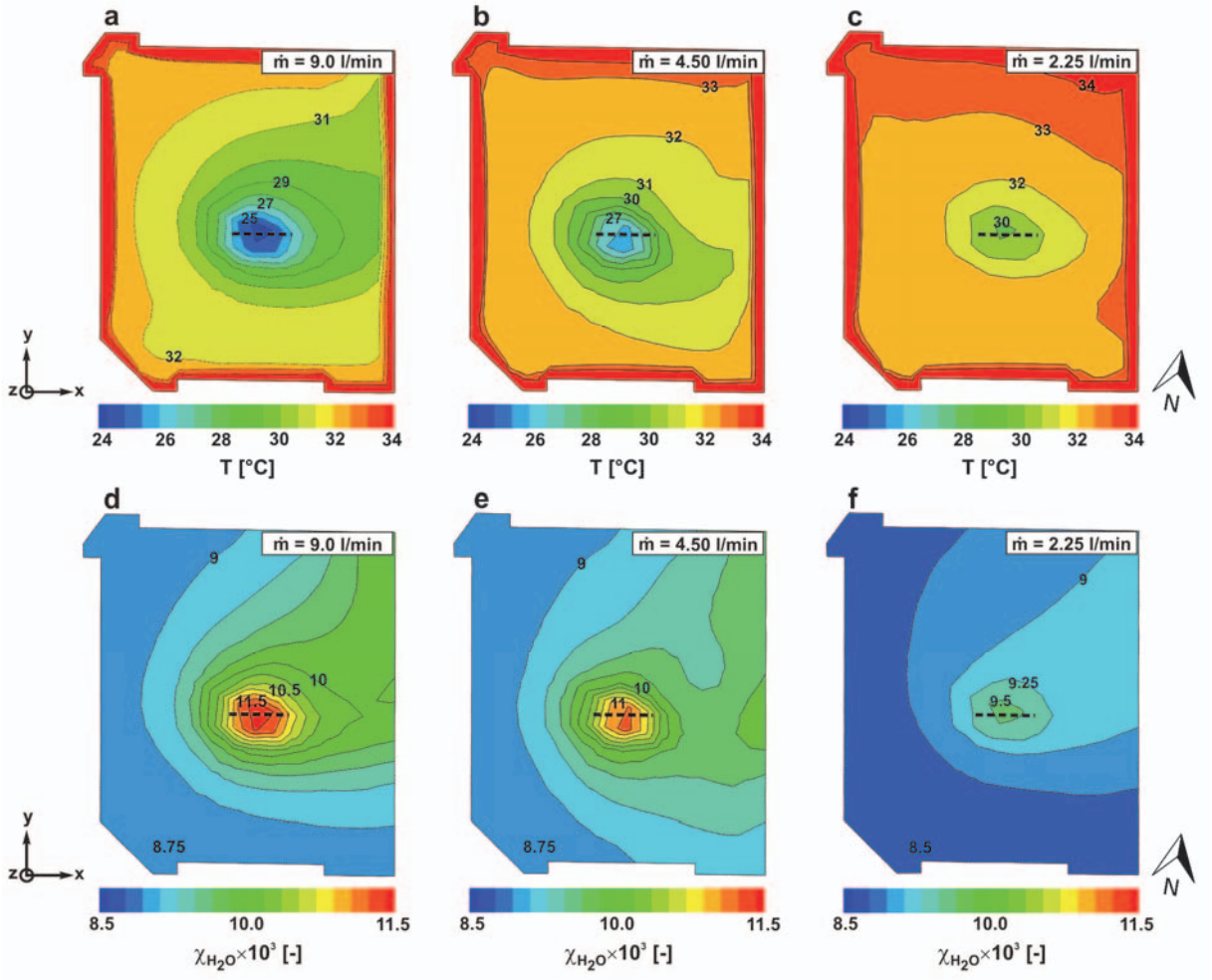

Fig. 13 Influence of water flow rate: air temperature distribution in a horizontal plane at a height of 1.75 m above ground level for (a) $\dot{m}_w$ = 9.0 l/min; (b) $\dot{m}_w$ = 4.50 l/min and (c) $\dot{m}_w$ = 2.25 l/min. (d-f) Same for vapor mass fraction (July 17, 2006: 12:00 h). The dashed line indicates the spray line.

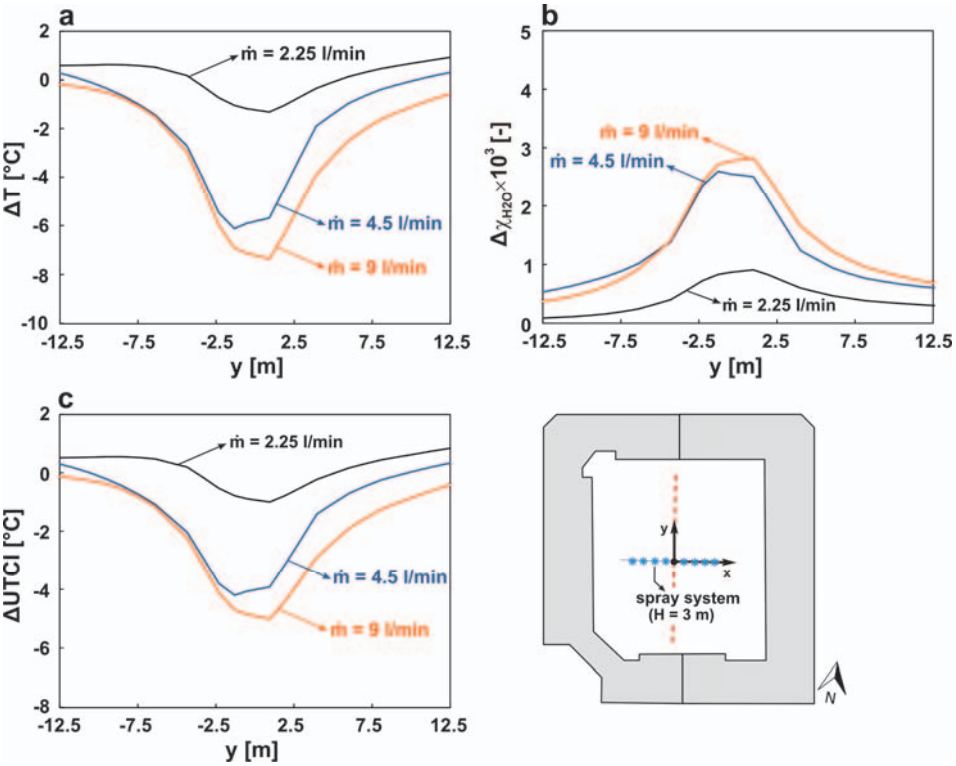

Fig. 14 Profiles of relative changes in (a) air temperature, (b) vapor mass fraction and (c) UTCI variations along line at height 1.75 m for different water flow rate $\dot{m}_w$.

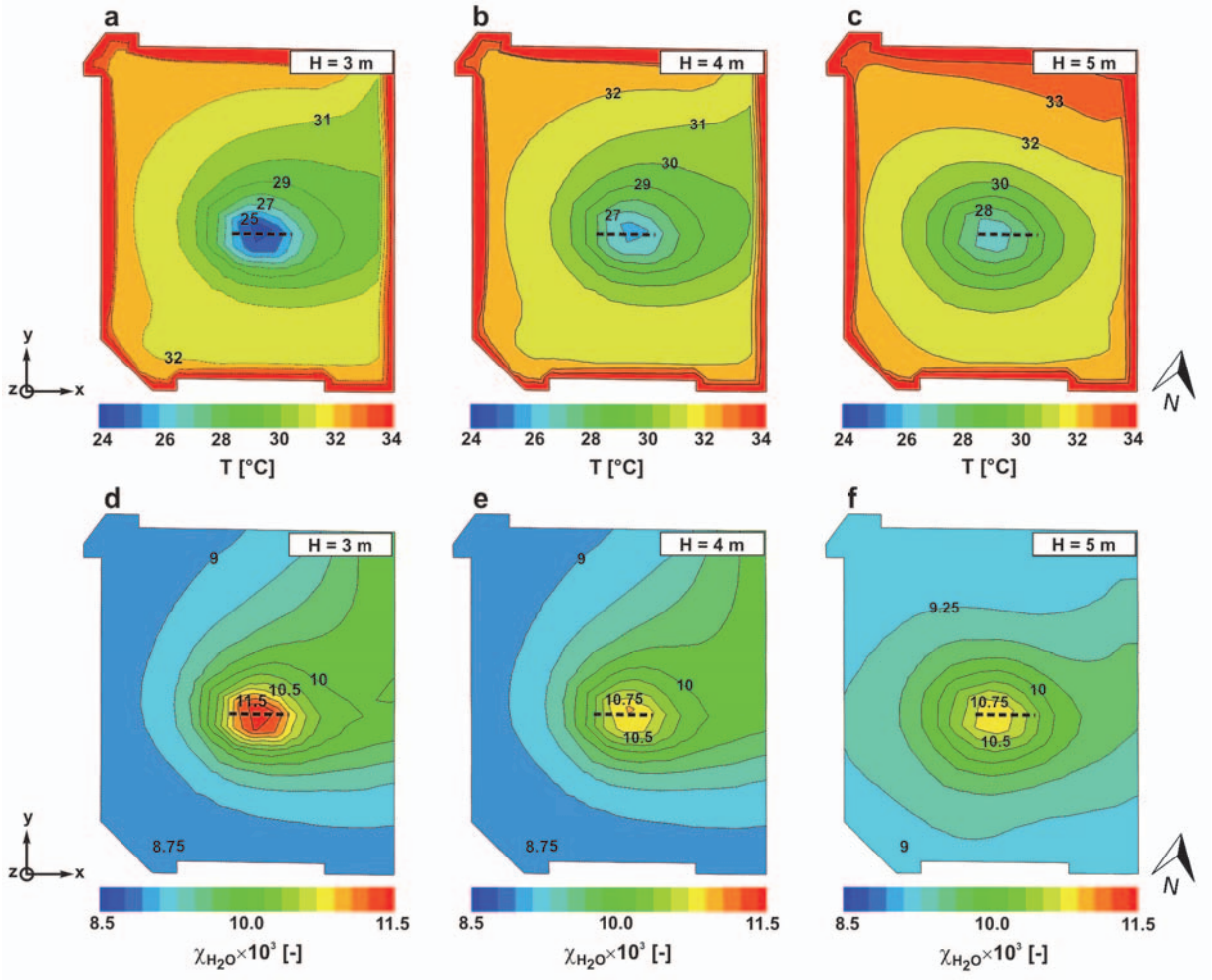

Fig. 15 Influence of height of spray system (H): air temperature distribution in a horizontal plane at a height of 1.75 m above ground level for (a) H = 3 m; (b) H = 4 m and (c) H = 5 m. (d-f) Same for vapor mass fraction (July 17, 2006: 12:00 h). The dashed line indicates the spray line.

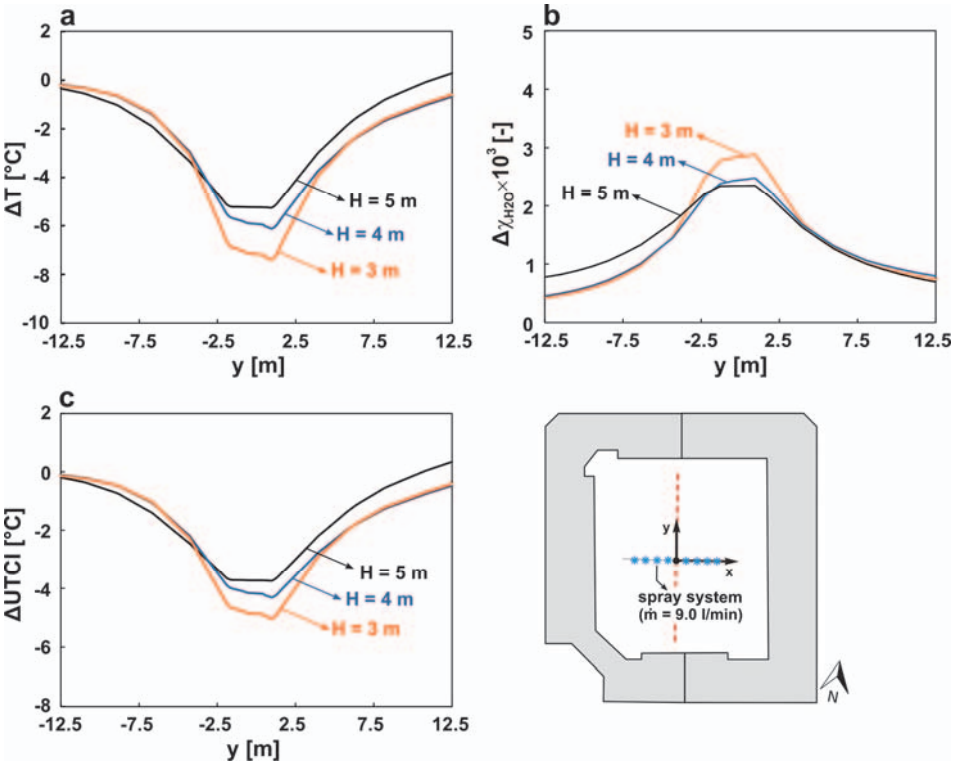

Fig. 16 Profiles of relative changes in (a) air temperature, (b) vapor mass fraction and (c) UTCI variations along line at height 1.75 m for different heights of spray system (H).

Tables

Table 1. List of some main parameters of the cases.

case	Inlet air			Water			Spray nozzle	
	V (m/s)	DBT (°C)	WBT (°C)	P (bar)	T_{in} (°C)	$\dot{m}$ (lit/min)	D (mm)	α/2 (deg.)
1	1	41.4	18.9	3	35.1	12.5	4.0	22.0
2	2	39.1	18.5	3	35.0	12.5	4.0	20.0
3	3	39.2	18.7	3	35.2	12.5	4.0	18.0

Table 2. Specifications of the materials used in this study.

Material	Density [kg/m^3]	Specific heat [J/kgK]	Thermal conductivity [W/mK]	Absorptivity	Emissivity
Earth	1150	650	1.5	0.60	0.90
Brick	1400	900	1.7	0.75	0.88

Table 3. List of main parameters of the cases including water velocity (V_w), temperature (T_w), flow rate ($\dot{m}_w$) and half-cone angle (α/2).

case	H [m]	V_w [m/s]	T_w [°C]	$\dot{m}_w$ [l/min]	α/2 [deg]	Droplet size distribution (Rosin-Rammler)				
						$\bar{D}$ [μm]	n	D_{min} [μm]	D_{max} [μm]	N
1	3	15	25	2.25	20	20	3.5	10	60	20
2	3	15	25	4.50	20	20	3.5	10	60	20
3	3	15	25	9.0	20	20	3.5	10	60	20
4	4	15	25	9.0	20	20	3.5	10	60	20
5	5	15	25	9.0	20	20	3.5	10	60	20

Table 4. UTCI equivalent temperature categorized in terms of thermal stress (Bröde et al., 2012).

UTCI range (°C)	Stress category
> 46	extreme heat stress
38 – 46	very strong heat stress
32 – 38	strong heat stress
26 – 32	moderate heat stress
9 – 26	no thermal stress
0 – 9	slight cold stress
-13 – 0	moderate cold stress
-13 – -27	strong cold stress
-27 – -40	very strong cold stress
< -40	extreme cold stress